Numerical simulation of non-Newtonian free shear flows

By G. M. Homsy [1] AND J. Azaiez [1]

1. Motivation and objectives

Free shear flows, like those of mixing layers, are encountered in aerodynamics, in the atmosphere, and in the ocean as well as in many industrial applications such as flow reactors or combustion chambers. It is, therefore, crucial to understand the mechanisms governing the process of transition to turbulence in order to predict and control the evolution of the flow. Delaying transition to turbulence as far downstream as possible allows a gain in energy expenditure while accelerating the transition can be of interest in processes where high mixing is desired. Various methods, including the use of polymer additives, can be effective in controlling fluid flows.

The drag reduction obtained by the addition of small amounts of high polymers has been an active area of research for the last three decades. It is now widely believed that polymer additives can affect the stability of a large variety of flows and that dilute solutions of these polymers have been shown to produce drag reductions of over 80% in internal flows and over 60% in external flows under a wide range of conditions. (Berman 1978, Sellin 1985 and Sellin & Moses 1989)

The major thrust of this work is to study the effects of polymer additives on the stability of the incompressible mixing layer through large scale numerical simulations. In particular, we focus on the two-dimensional flow and examine how the presence of viscoelasticity may affect the typical structures of the flow, namely roll-up and pairing of vortices.

2. Accomplishments

2.1 Problem definition

The flow is examined in a reference frame moving with the average velocity. In such frame, the flow is characterized by the upper free-stream velocity u_o and the momentum thickness of the mixing layer δ. We used a vorticity-streamfunction formulation for Cauchy's momentum equation,

$$\rho \frac{D\vec{v}}{Dt} = -\nabla p + \nabla \cdot \boldsymbol{\tau} \tag{1}$$

This equation is closed through evolution equations relating the stress tensor to the shear rate tensor. In all the subsequent analysis, the stress tensor is written as the sum of two terms (Larson (1988) and Bird *et al.* (1987)):

$$\boldsymbol{\tau} = \boldsymbol{\tau}^s + \boldsymbol{\tau}^p = \eta_s \dot{\boldsymbol{\gamma}} + \eta_p \mathbf{a} = \eta[\kappa \dot{\boldsymbol{\gamma}} + (1-\kappa)\mathbf{a}] \tag{2}$$

1 Stanford University

The first term corresponds to the contribution of the Newtonian solvent and is proportional to the shear rate tensor with η_s the solvent viscosity. The second term represents the polymeric contribution to the stress, and is proportional to the tensor **a** with η_p the polymeric contribution to the shear viscosity. The parameter $\kappa = \dfrac{\eta_s}{\eta_s + \eta_p} = \dfrac{\eta_s}{\eta}$ may vary between 0 and 1. When $\kappa = 1$, the field equations and the constitutive equations can be decoupled, and the problem reduces to that of purely Newtonian flow.

The tensor **a** satisfies the appropriate rheological equation that can be of differential or integral form (Bird 1967). In the present study, we used two rheological models, the Oldroyd-B model and the FENE-P model.

2.2 Rheological models

In the Oldroyd-B model, the polymer stress **a** satisfies the upper convected Maxwell equation:

$$\lambda \frac{\delta \mathbf{a}}{\delta t} + \mathbf{a} = \dot{\boldsymbol{\gamma}} \tag{3}$$

where:

$$\frac{\delta \mathbf{a}}{\delta t} = \frac{\partial \mathbf{a}}{\partial t} + \vec{v} \cdot \nabla \mathbf{a} - \nabla \vec{v}^{\perp} \cdot \mathbf{a} - \mathbf{a} \cdot \nabla \vec{v} \tag{4}$$

is the upper-convected derivative of **a**, and λ is the relaxation time of the polymer. This model gives a reasonably good qualitative description of dilute polymer solutions, but unfortunately, it gives rise to a steady state elongational viscosity that diverges at a finite elongational rate. This unlikely behavior results from the infinite extensibility of the linear Hookean spring used to model the polymer. In order to avoid this problem, a nonlinear spring based on Warner law can be used to describe the finite extensibility of the polymer, leading to the FENE-P model. This model is best formulated in terms of the tensor $\mathbf{B} = \dfrac{H\langle \mathbf{RR} \rangle}{kT}$ where $\langle \mathbf{RR} \rangle$ is the configuration tensor, H the spring constant, k the Boltzmann constant, and T the absolute temperature. The tensor **B** satisfies the following equation:

$$Z\mathbf{B} + \lambda \frac{\delta \mathbf{B}}{\delta t} = \mathbf{I} \tag{5}$$

In Eq. (5), **I** is the unit tensor and $Z = (1 - \langle \dfrac{R^2}{{R_o}^2} \rangle)^{-1} = (1 - \dfrac{tr\mathbf{B}}{b})^{-1}$. The parameter $b = \dfrac{H{R_o}^2}{kT}$, where R_o represents the maximal possible extension of the polymer, is a measure of the extensibility of the polymer chain. An equivalent formulation of Eq. (5) in terms of the tensor **a** can be obtained using the transformation:

$$\mathbf{a} = \frac{Z\mathbf{B} - \mathbf{I}}{\lambda} \tag{6}$$

2.3 Scaling and parameters

Using u_o and δ as the reference velocity and the reference length, respectively, the flow is characterized by the Reynolds number, $Re = \frac{\rho \delta u_o}{\eta} = \frac{\delta u_o}{\nu}$, where ν is the kinematic viscosity of the fluid, and the Weissenberg number, $We = \frac{\lambda u_o}{\delta}$, is a dimensionless measure of the relaxation time of the polymer. The elasticity number $E = \frac{We}{Re} = \frac{\lambda \nu}{\delta^2}$ is often used to characterize the elasticity of the fluid. In addition to Re and We, κ and, in the case of the FENE-P model, b are the other model parameters.

2.4 Numerical method

The simulations reported in this study were performed by solving the vorticity equation:

$$[\frac{\partial}{\partial t} - \frac{\kappa}{Re}\nabla^2]\omega = -[u\frac{\partial}{\partial x} + v\frac{\partial}{\partial y}]\omega + \frac{(1-\kappa)}{Re}[(\frac{\partial^2}{\partial x^2} - \frac{\partial^2}{\partial y^2})a_{12} - \frac{\partial^2}{\partial x \partial y}(a_{22} - a_{11})] \quad (7)$$

coupled with the appropriate stress equations. In the present study, we are interested in the forced, temporally growing mixing layer. The initial flow is composed of the viscously spreading *tanh* vorticity profile and the corresponding base-state polymer stress, seeded with the wave that, according to linear stability analysis (Azaiez & Homsy 1993), has the largest growth rate.

The dynamical equations are solved using a pseudo-spectral method in which the flow variables are expanded in a modified Hartley series (Zimmerman & Homsy (1991)). The resulting set of ordinary differential equations is advanced in time using an operator splitting algorithm (see *e.g.* Tan & Homsy (1987)). In addition to those with the spectral code, a few simulations have been conducted using a finite difference scheme second order accurate in space and in time. A description of the scheme can be found in the paper by Orlandi *et al.* (1992). The results obtained from these two codes were always in total concordance. The codes were validated by comparing with the linear stability results (Azaiez & Homsy (1993)) and by checking that they reproduced the same results as the Newtonian code when we set $\kappa = 1$.

A typical run for the roll-up of the non-Newtonian fluid required 128x128 spectral modes and a time step $\Delta t = 0.04$. This resolution gives satisfactory results at moderate values of the Weissenberg number and was refined for large values of We. Throughout this study, the value of the parameter κ is fixed to 0.5.

3. Results

3.1 The Oldroyd-B model

The vorticity and stress equations for the Oldroyd-B model have been solved numerically for various values of We, and for Re =100. For small values of We ($We \sim 1$), the flow does not show any noticeable changes from the Newtonian case. Numerical simulations at moderately high We ($We \sim 10$) developed an instability that

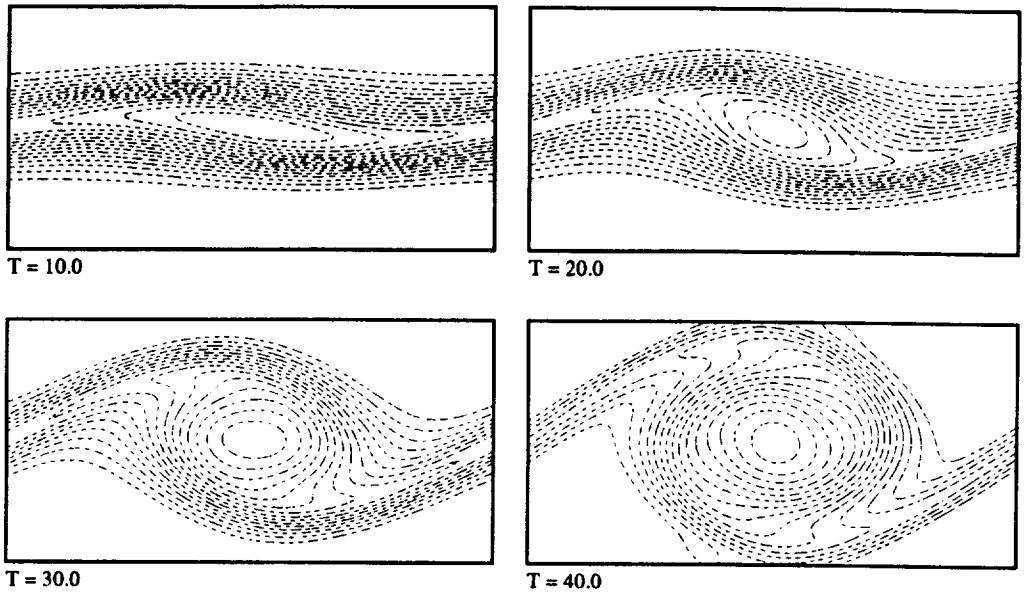

FIGURE 1. Vorticity contours for Re=100.

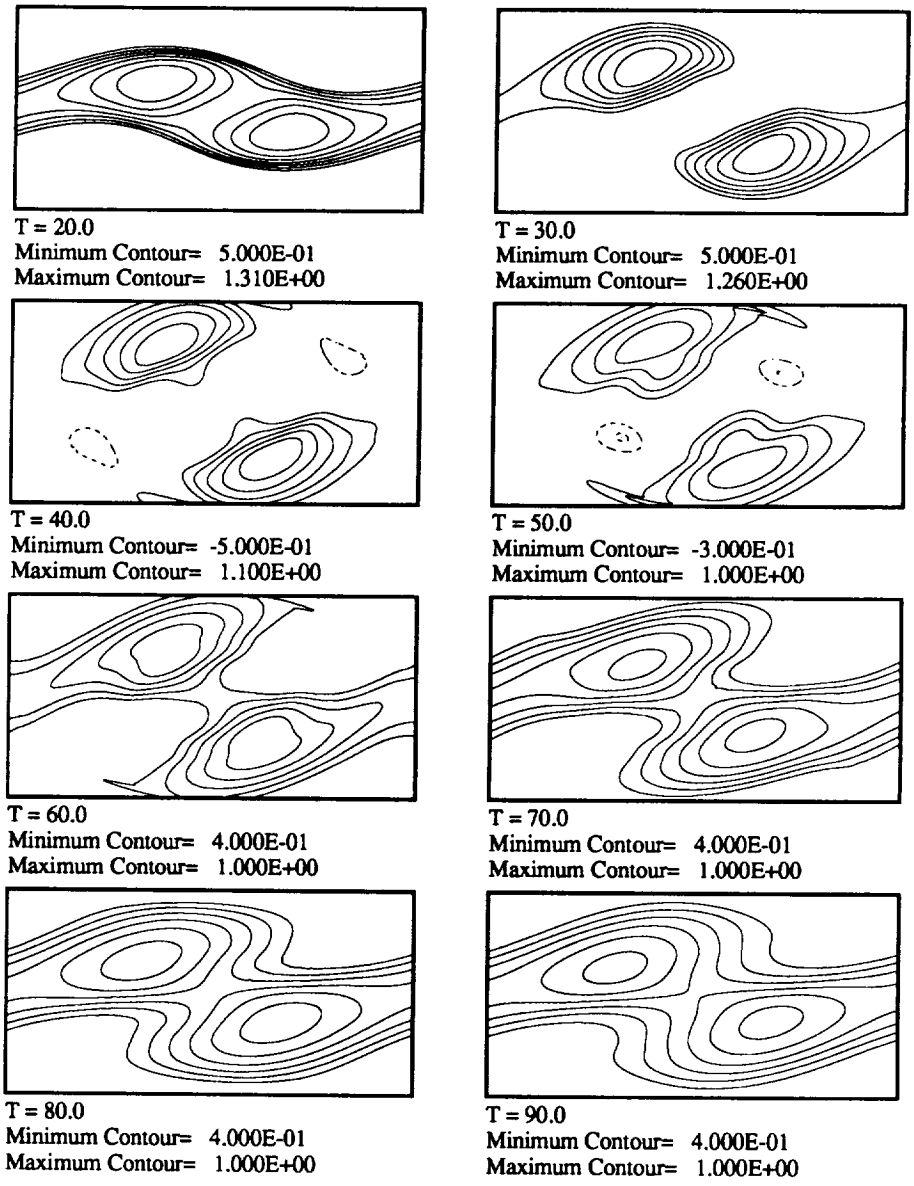

FIGURE 2. (B11 -B22) contours for FENE-P model. Re=50, E=0.5, and b=5.

lead to the divergence of the code. We examined the origin of this instability by looking at the evolution of the different terms in the polymer stress equations. The analysis of these terms showed that the instability is associated with a deficiency of the Oldroyd-B model that allows stresses to grow indefinitely. The instability starts to develop first in the braid regions where the product of the Weissenberg number and the dimensionless local extensional rate exceeds unity. In these regions, and due to high extensional rates, the chain is stretched rapidly, and because of its large relaxation time associated with the high We, it is prevented from coiling up as quickly as its stretching. As a consequence, the chain gets extended indefinitely and the stresses grow exponentially. The intense build-up of the stresses ultimately leads to the divergence of the numerical code.

3.2 The FENE-P model

Unlike the Oldroyd-B model, the FENE-P model does not allow infinite extension of the spring used to model the polymer, and as we have seen, the maximal extension of the spring is characterized by the parameter b. The viscoelastic mixing layer has been successfully simulated for various values of the three parameters, Re, E, and b. In what follows, we describe results for the two mechanisms of instability of the two-dimensional mixing layer, namely the roll-up and the pairing of the flow.

3.2.1 Roll-up

We explored values of the Reynolds number between 50 and 400, varied the Weissenberg number between 20 and 200, and examined values of b between 1 and 20. Figure 1 shows a time sequence of the roll-up of the flow for the Newtonian case and for the FENE-P model. As it has been experimentally documented (Riediger 1988), we observed a trend for smaller values of the minimal (negative) vorticity in the case of the viscoelastic flow, as well as a tendency for the vortex structures to be more compact and to have longer life times than in the Newtonian fluid. The global structure of the flow as well as the roll-up time are basically the same for both fluids. However, the local distribution of the vorticity is affected by the presence of the viscoelasticity in the flow with high gradients tending to appear in some parts of the flow, namely in the braids. The evolution of the absolute value of the minimal vorticity at various streamwise locations confirms the conclusion of the tendency to have *more spanwise vorticity remaining in the braid region.*

The examination of contours of the first normal polymer stress $(B_{11}-B_{22})$ showed that there is a spatial correlation between the regions of intensification of the vorticity gradients and those where there is a build-up of the first normal polymer stress.

In order to understand the reasons why the global structure of the roll-up remains unchanged, we examined the evolution of the polymer stresses in connection with that of the vorticity (Figure 2). This study revealed that the first normal stresses reach a quasi-steady state characterized by the absence of any extensional forces and a balance between shearing forces and the polymer relaxation stresses, and it is interesting to note the spatial relationships between vorticity and normal stresses that characterize this quasi-steady state. After the first stage of roll-up, most of the

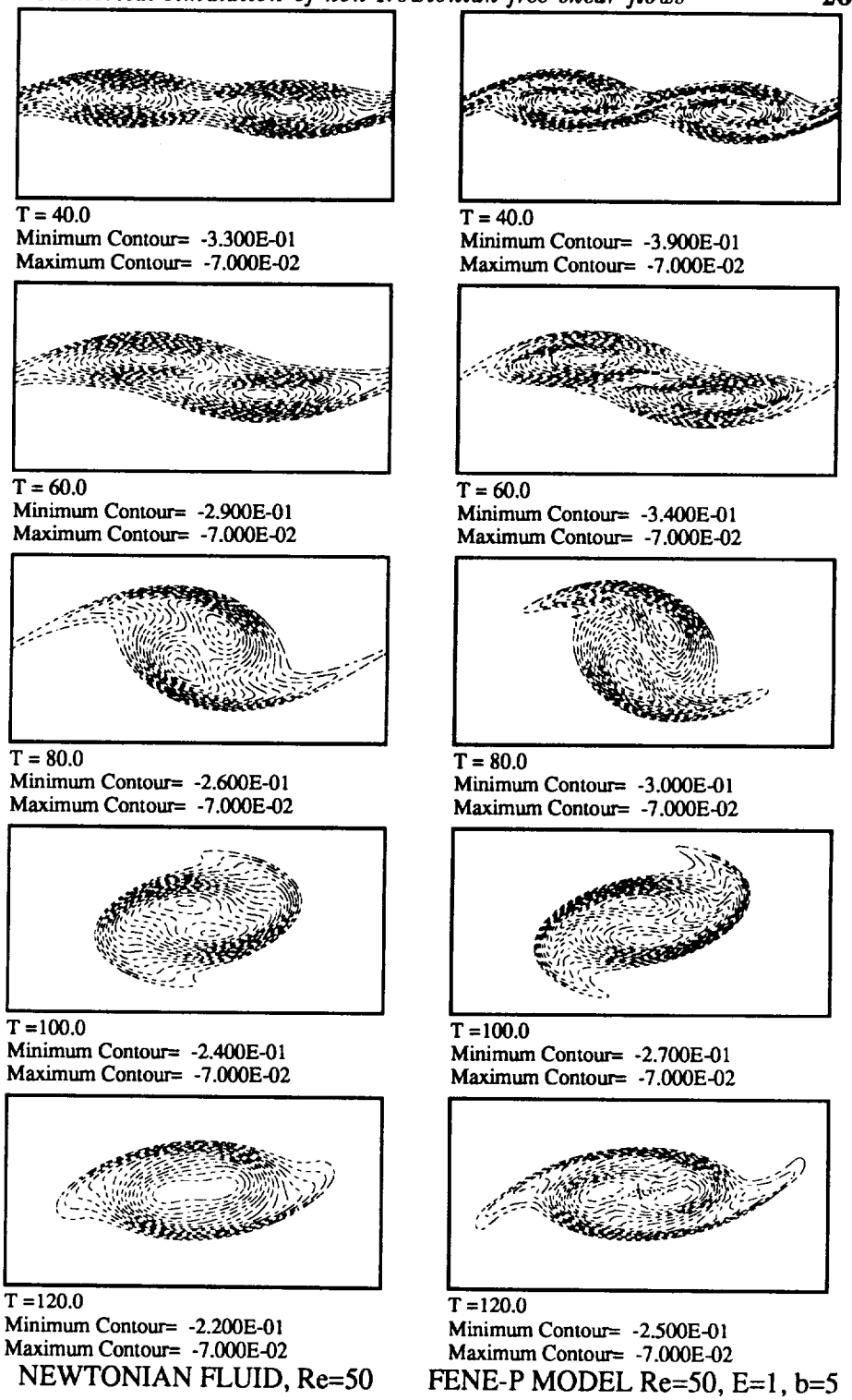

FIGURE 3. Vorticity contours for FENE-P model. Re=50, E=1, and b=2.

vorticity is entrained into the vortex core with only little remaining in the braids, while the stress fields are highest in regions of highest shear, which tend to lie in nearly irrotational regions surrounding the vortex core. This feature may be key to explaining why the global flow structure is unaffected by viscoelasticity.

Simulations at various values of the parameters E and b show that the establishment of the steady state for $(B_{11} - B_{22})$ is, at least for the range of E and b examined, a common trend of the evolution of the polymer stresses in free shear flows and is insensitive to the value of E or b. A detailed discussion of this steady state is found in the article by Azaiez & Homsy (1994)

3.2.2 Pairing

We examined the pairing of the flow for $Re = 50$ and various values of E and b. In the bulk of the simulations, we used 256 grid points in the streamwise direction and 128 grid points in the transverse direction and a time step $\Delta t = 0.02$. Simulations at large E ($E \sim 2$) required a finer resolution and we used 256x256 spectral modes and a time step $\Delta t = 0.01$. Figure 3 shows a time sequence of the vorticity contours for the Newtonian fluid with Re=50 and the non-Newtonian fluid with $Re = 50$, $E = 1$ and $b = 5$. In the early stage, the flow shows the same trends for intensification of the vorticity that we have encountered in the case of the single roll-up. Later the two vortices start their orbital motion, with the tendency for a slightly faster rotational motion in the case of the viscoelastic fluid. Note that during roll-up as well as pairing, the vortices are more diffuse in the case of the Newtonian fluid and that the maximal absolute value of the vorticity over the whole flow is larger for the viscoelastic fluid. We attribute the faster rotation of the two parent vortices around each to the vorticity gradients that develop in the braids during the roll-up of the flow. These gradients lead to a stronger outer field between the two parent vortices that enhances the mutually induced rotational motion of the two vortices (Azaiez & Homsy (1994))

4. Conclusion

In the present study, we examined the instability of the plane, incompressible, non-Newtonian mixing layer, focusing on simulations with high Re and We. Numerical simulations using the Oldroyd-B model developed an instability for moderate We. We examined the origin of this instability by looking at the evolution of the different terms in the stress equations, which showed that the instability is associated with a deficiency of the Oldroyd-B model that allows stresses to grow indefinitely. The instability starts to develop first in the braid regions where the product of the Weissenberg number and the local extensional rate is larger than one is larger than one. The unbounded growth and intense build-up of the stresses ultimately leads to the divergence of the numerical code. Most of the numerical simulations have been performed with the FENE-P equations which revealed to be the most appropriate model for the simulation of free shear flows at high elasticity. These simulations showed that, for the range of parameters examined, the global structure of the flow as well as the roll-up and pairing times are unchanged from the Newtonian case. However, local vorticity intensifications associated with the build-up

of normal stresses have been observed in the braids as well as in the vortex core. As it has been experimentally documented (Riediger 1988), we observed a trend for smaller values of the minimal (negative) vorticity in the case of the viscoelastic flow as well as the tendency for the vortex structures to be more compact and to have longer life times than in the Newtonian fluid.

The examination of the evolution of the first normal stresses revealed a very interesting steady state characterized by the absence of any extensional forces and a balance between shearing forces and the polymer relaxation stresses.

Acknowledgements

The authors would like to acknowledge useful discussions with Professor E. J. Hinch from Cambridge University and Professor P. Orlandi from the University di Roma. They also thank Professor E. S. G. Shaqfeh for his helpful comments and suggestions.

REFERENCES

AZAIEZ, J., & HOMSY, G. M. 1993 Linear stability of free shear flows of viscoelastic liquids. Submitted to *J. Fluid Mech.*

AZAIEZ, J., & HOMSY, G. M. 1994 Numerical simulation of non-Newtonian free shear flows at high Reynolds numbers. Submitted to *J. Non-Newtonian Fluid Mech.*

BERMAN, N. 1978 Drag Reduction by Polymers. *Ann. Rev. Fluid Mech.* **10,** 47-64.

BIRD, R. B. 1976 Useful non-Newtonian Models. *Ann. Rev. Fluid Mech.* **8,** 13-34.

BIRD, R. B., CURTISS, C. F., ARMSTRONG, R. C. & HASSAGER, O. 1987 *Dynamics Polymeric Liquids*, vol. 2, 2nd edn. Wiley-Intersciences.

LARSON, R. G. 1988 *Constitutive Equations for Polymer Melts and Solutions*, Butterworths Series in Chemical Engineering.

ORLANDI, P., HOMSY G. M., & AZAIEZ, J. 1992 Direct simulation of polymer drag reduction in free shear flows and vortex dipoles. *Proceedings of the 1992 Summer Program.* Center for Turbulence Research, NASA Ames-Stanford University.

RIEDIGER, S. 1989 *Drag Reduction in Fluid Flows*, Ellis Horwood Limited, 303-310.

SELLIN, R. H. J. 1985 Industrial Applications for Drag Reducing Polymer Additives: A review *Proceedings of the third International conference on drag reduction.* Bristol.

SELLIN, R. H. J. & MOSES, R. T. 1989 *Drag Reduction in Fluid Flows.* Ellis Horwood-Publishers.

TAN, C. T. & HOMSY G. M. 1987 Simulation of nonlinear viscous fingering in miscible displacement. *Phys. Fluids.* **31,** 1330-1338.

ZIMMERMAN, W. B. & HOMSY, G. M. 1991 Nonlinear viscous fingering in miscible displacement with anisotropic dispersion. *Phys. Fluids A.* **3** 8, 1859-1872.